SEP

AFRL-SR-BL-TR-01-

0485

REPORT DOCUMENTATION PAGE

Public reporting burden for this collection of information is estimated to average 1 hour per response, including the time for reviewing ins
the data needed, and completing and reviewing this collection of information. Send comments regarding this burden estimate or any oth
reducing this burden to Department of Defense, Washington Headquarters Services, Directorate for Information Operations and Reports
VA 22202-4302. Respondents should be aware that notwithstanding any other provision of law, no person shall be subject to any penalty for failing
display a currently valid OMB control number. **PLEASE DO NOT RETURN YOUR FORM TO THE ABOVE ADDRESS.**

1. REPORT DATE (DD-MM-YYYY)	2. REPORT TYPE	3. DATES COVERED (From - To)
09/06/2001	Final Report	Apr 2000 – Mar 2001

4. TITLE AND SUBTITLE
Instrumentation to Support PIV and HPIV Measurements in an Axial
Turbomachine Flow Visualization Facility

5a. CONTRACT NUMBER

5b. GRANT NUMBER
F49620-00-1-0199

5c. PROGRAM ELEMENT NUMBER

6. AUTHOR(S)
Katz, Joseph and Meneveau, Charles

5d. PROJECT NUMBER

5e. TASK NUMBER

5f. WORK UNIT NUMBER

7. PERFORMING ORGANIZATION NAME(S) AND ADDRESS(ES)

The Johns Hopkins University
Department of Mechanical Engineering
3400 N. Charles St.
Baltimore, MD 21218

8. PERFORMING ORGANIZATION

20011005 129

9. SPONSORING / MONITORING AGENCY NAME(S) AND ADDRESS(ES)
Air Force Office of Scientific Research
801 North Randolph Street
Arlington VA, 22203-1977

10. SPONSOR/MONITOR'S ACRONYM(S)
AFOSR/NA

**11. SPONSOR/MONITOR'S REPORT
NUMBER(S)**

12. DISTRIBUTION / AVAILABILITY STATEMENT

13. SUPPLEMENTARY NOTES

14. ABSTRACT
This DURIP grant has provided instrumentation that supports an AFOSR sponsored program. The objective of this program is to measure the unsteady flow in axial turbomachines and use the data to address turbulence and flow modeling issues that are specific to such complex environments. The motivation is to examine turbulence and unsteady flow phenomena at three levels of modeling: Passage-averaged, steady RANS, unsteady RANS, and subgrid scale stress modeling for LES. The report describes in detail our unique two-stage axial-turbomachine flow visualization facility, specifying the instruments purchased under the present grant and how they fit into the system. This facility contains fluid (concentrated solution of NaI in water) with an optical index of refraction that matches that of the acrylic blades of the second stage. Consequently, it allows unobstructed view on an entire stage including the rotor, stator and the gaps between blade rows. Two and three dimensional velocity measurements can be performed using 2-D Particle Image Velocimetry, planar 3-D measurements using stereo-PIV and full 3-D HPIV. The report also describes current 2-D PIV measurements and presents sample data. With available access to any desired plane, these measurements provide data on rotor-stator interactions, the effects of wakes on downstream blades, tip leakage flows and hub vortices and their interactions with neighboring blades, unsteady separation, particularly off-design conditions, etc.

15. SUBJECT TERMS
Particle Image Velocimetry, turbomachines, Deterministic Stresses, Turbulence

16. SECURITY CLASSIFICATION OF:			17. LIMITATION OF ABSTRACT	18. NUMBER OF PAGES	19a. NAME OF RESPONSIBLE PERSON Joseph Katz
a. REPORT	b. ABSTRACT	c. THIS PAGE	UU		19b. TELEPHONE NUMBER (include area code)
U	U	U		24	410-516-5470

Standard Form 298 (Rev. 8-98)
Prescribed by ANSI Std. Z39.18

Instrumentation to Support PIV and HPIV Measurements in an Axial Turbomachine Flow Visualization Facility

Final Report

Submitted By

Joseph Katz and Charles Meneveau

Department of Mechanical Engineering
The Johns Hopkins University
Baltimore, MD 21218

Executive summary

This DURIP grant provided instrumentation that supports an AFOSR sponsored program (grants #F49620-97-1-011 and # F49620 – 01 – 1 – 0010). The objective of this program is to measure the unsteady flow in axial turbomachines and use the data to address turbulence and complex flow modeling issues that are specific to such complex environments. This report has three sections. The first (Section 1) briefly provides the motivation for the present study. The objective is to examine turbulence and unsteady flow phenomena at three levels of modeling: (i) Passage-averaged, steady RANS (Adamczyk, 1985), presently used for multiple blade-row simulations; (ii) Unsteady RANS, and (iii) subgrid scale (SGS) stress modeling for Large-Eddy-Simulation (LES). The second section describes a unique two-stage axial-turbomachine flow visualization facility, specifying the instruments purchased under the present grant and how they fit into the system. This facility contains fluid (concentrated solution of NaI in water) with an optical index of refraction that matches that of the acrylic blades of the second stage. Consequently, it allows unobstructed view on an entire stage including the rotor, stator and the gaps between blade rows. Two and three dimensional velocity measurements can be performed using 2-D PIV (Particle Image Velocimetry), planar 3-D measurements using stereo-PIV and full 3-D HPIV (Holographic PIV). The third section describes 2-D PIV measurements that are presently in progress and provides sample data. With available access to any desired plane (or volume), these measurements will provide quantitative information on rotor-stator interactions, such as the effects of wakes on downstream blades, tip leakage flows and hub vortices and their interactions with neighboring blade rows, unsteady separation, particularly off-design conditions, etc.

1.0 Objectives and Scientific Motivation

Flows in turbomachines, i.e. compressors, turbines, and pumps, are three-dimensional, complex and unsteady. These flow phenomena dominate the performance, efficiency, noise, and vibrations of these machines, and as a result must be understood and accurately predicted. The scientific objectives are best understood within the context of modeling, as outlined in this Section. Tools for quantitative flow predictions in multi-stage turbomachinery have evolved considerably over the past few decades. Numerical simulation techniques are playing a role of growing significance in improving stage and overall efficiency during design, as well as in understanding complex flow-phenomena. An abbreviated list of these techniques is given below, in a sequence that roughly follows their chronology and their level of complexity.

1.1 Throughflow techniques: This steady, 2-D, 'traditional' simulation tool for multi-stage designs is based on solving axisymmetric problems, where the circumferential variations are averaged out (Adkins & Smith, 1982; Gallimore & Cumpsty, 1986). Non-axisymmetric effects have to be modeled using empirical correlations that account for blockage and mixing effects of blades, tip leakage, hub vortices and wakes. A concomitant problem of these models is that they work only near conditions for which they have been calibrated, typically near design conditions. While this approach is often complemented with limited, 2-D simulations of axisymmetric stream surfaces (or some single-stage 3-D calculations), it has difficulties dealing with three-dimensionalities and interactions between rows (see e.g. Dawes, 1992).

1.2 Passage-averaged 3-D Methods: This approach solves the steady, three-dimensional equations (Euler, or Reynolds-averaged Navier-Stokes -- RANS) separately in one (or a few) passage, in each of the blade rows of a multistage machine. Such steady 3D simulations are

3

starting to be considered affordable for actual design purposes, even when a large number of stages is involved. Unsteady effects caused by neighboring rows are averaged out in the circumferential direction, and this information is passed along, from one row to another. There are basically two methods for transferring this information. The first is the "mixing plane approach" (e.g. Dawes, 1992; Denton, 1992), in which information is passed along as a boundary condition on a plane between blade rows. Although more accurate than through-flow techniques, it is very difficult to match all the parameters at the interface, resulting in discontinuities. The second and improved method is "the average-passage approach" (Adamczyk, 1985; Adamczyk et al., 1990; Rhie et al., 1998; LeJambre et al., 1998; Busby et al., 2000). Here the computational domain of a given row is extended to include the volume occupied by neighboring rows, but not the blades. The flow-turning effect associated with the blades (pressure difference across a surface) is introduced through steady body-forces, while the effects of the unsteady velocity field is introduced through "deterministic" stresses. This approach is more rigorous than the mixing plane method since it provides a framework for accounting for the effects of unsteady phenomena on the time averaged flow field. These effects cannot be accounted for by steady boundary conditions.

While the average-passage approach is very useful and affordable for design purposes, important modeling problems associated with unsteady interactions between blade-rows arise. In terms of modeling, in many current applications a frozen blade wake is swept through the field of the following row, and averaged. Consequently, unsteady interactions between blade rows are not accounted for. For example, in Sinha et al. (2000a, b) we show how unsteady incidence angles resulting from the passage of rotor blades generate cyclic flow separations on the leading edge and mid sections of the stator blades. The rotor passage also alters the wakes of the diffuser vanes and the proximity to the stator vanes alters the structure of rotor wake. The effect of wake unsteadiness is considered in Adamczyk et al. (1996). A deterministic stress model based on solving the unsteady Euler Equations (i.e. inviscid flow) has been recently introduced in Busby et al. (2000). Since the deterministic stresses are typically of similar or higher magnitude than the Reynolds stresses (Rhie et al., 1998, Le Jambre et al. 1998; Kirtley et al. 1993, and Sinha et al., 2000b), neglecting these interactions in simulations may lead to significant errors. Experimental data to determine these deterministic stresses is critical to guide and test new model developments. We have generated such data at high spatial and temporal resolution, previously in our centrifugal facility Sinha et al. (2000a, b, 2001), and in the present measurements, in the new axial facility. We have also introduced another method to model the deterministic stresses, which compares favorably with the experimental data (Meneveau and Katz, 2001).

1.3 Phase-averaged unsteady RANS: This method involves two simulations of one or a few passages, one in the rotor frame and the other in the stator frame of reference. They are coupled by unsteady boundary conditions arising from sweeping the outlet plane of one solution past the inlet plane of the other (see e.g. Rai, 1987; Lakshminarayana, 1991; Survamshiya and Lakshminarayana, 1995, Ho and Lakshminarayana, 1995 and many others). This approach is currently limited to single-stage computations, since simulations of multi-stage configurations are prohibitive, especially when blade-counts vary from one stage to the next (complicating the phases that would have to be considered). Thus, it is understood that unsteady RANS of an entire multistage compressor is not on the horizon. This limitation justifies a continued interest in modeling issues of the average-passage technique. The usefulness of unsteady RANS in this

context is in a way similar to the experimental data: It provides detailed data on the flow structure within a limited subsection of the turbomachine. The difficulty with unsteady RANS is the modeling of Reynolds stresses. Currently no consensus exists as to which of the many Reynolds stress models (simple k-ε, RNG-k-ε, second-order modeling, algebraic stress, low Reynolds-number corrections, etc.) is best suited for turbomachine applications (Lakshminarayana, 1991). Although modeling of unsteady RANS is not the primary focus of this project, still, we are mapping 2-D spatial and temporal distributions of the phase-averaged Reynolds stresses on several planes along with the unsteady flow structure. This data will be made available for code validation. We will also compare the Reynolds stresses to the deterministic stresses.

Turbulence modeling problems in unsteady RANS, especially in the complex environment of a turbomachine, create uncertainties associated with the validity of the results. The primary difficulties are caused by the fact that all the turbulence, including eddies with sizes comparable to an entire vane passage, must be modeled. Since these eddies do not have a universal structure (e.g. Wilcox, 1993; Speziale, 1991), it is necessary to adjust the models on a case-by-case basis, which reduces their effectiveness as a predictive tool. These difficulties have led to development of a wide variety of RANS models with varying complexity that are beyond the present scope. These models have led to significant improvements but not to breakthroughs. Consequently, to provide fundamentally more accurate simulations of turbulent flows in complex environment, it is of interest to explore the application of Large-Eddy simulations.

1.4 Large-Eddy-Simulation (LES): This approach does not average out random fluctuations associated to turbulence, but only smears out small-scale fluctuations (Rogallo & Moin, 1984, Lesieur & Metais, 1996; Meneveau & Katz, 2000). Spatially filtered, unsteady Navier-Stokes equations (LES equations) are solved to capture not only the unsteadiness associated with relative motion between rotor and stator, but also to resolve random motion of large-scale turbulent eddies, such as large eddies in wakes, meandering of tip-leakage and hub vortices, etc. Phase-averaged data is then determined by averaging the results. The spatial resolution does not need to approach viscous (Kolmogorov) length-scales because of the filtering. For now, a practical limitation of LES is that its computational cost is orders of magnitudes larger that RANS, mainly due to much longer integration times needed to achieve converged statistics. However, rapid increases in computer power are raising the expectation that LES may soon become practical even in complex turbomachine environments. More fundamentally, the filtering introduces "subgrid-scale" (SGS) stresses that account for the mixing and kinetic energy dissipation by the unresolved, small-scale fluctuations. Small-scale fluctuations in the inertial range of turbulence are known to be less flow dependent than the large-scale eddies, thus raising the hope for more "universal" models. There has already been considerable effort in development of LES models and applications to various basic flows, and some of increasing complexity.

Our group has experimentally examined several issues related to SGS modeling in relatively simple flows, such as homogeneous turbulence (Meneveau, 1993), the far-field of a round jet (Liu et al., 1994, 1995), in a cylinder wake (O'Neil & Meneveau, 1997), during rapid axisymmetric expansion (Liu et al., 1999), and within a square duct (Zhang et al., 1997, Tao et al., 1999, 2000, 2001). Considerable portion of this effort has involved implementation of PIV to

generate the data-bases and some of the analysis has been based on hot wire data. The experiments and analysis in Tao et al. (1999, 2000, 2001) already involve use of HPIV to obtain full 3-D velocity distributions (130x130x130 vectors) in a finite volume (4.5x4.5x4.5 cm^3). These data are filtered at different spatial scales, which allows us to compare between large (resolved scales) and small scales (subgrid stresses). As reviewed in Meneveau & Katz (2000), the basic modeling paradigm that has been established by our work is the use of computed large-scales to locally guide the modeling at small scales. We learned from simpler flows that model coefficients must be modified when turbulence is exposed, for example, to rapid straining or when the filter scale approaches the integral scale. The available data indicates that such modifications can be determined from the response of the resolved structures to the local flow. LES, unlike RANS, allows us to perform "dynamic" modifications to the modeling, since part of the turbulence is resolved. When applying LES to the unsteady flow in a blade-passage, there is a need to implement much more refined models to account for different flow regimes.

As described in Sinha et al., (2000a, b), we have used PIV data in a centrifugal pump with a vaned diffuser to directly measure the relevant large-scale, filtered flow structure, the distribution of subgrid-scale stresses and the associated kinetic energy dissipation. Interesting phenomena, such as regions with consistent energy backscatter (from small scales to large scales) have been identified. We also find, consistent with results from simple geometries, that eddy-viscosity models are inherently deficient. Filtering of the data at various scales (provided the data has sufficient resolution) should enable us to compare the response of different scales to the external forcing, and incorporate the measured behavior into improved modeling. We plan to perform these measurements in the new axial flow facility described in the next section.

2. Axial Flow Facility

2.1 Rationale for the Selected System: Providing answers to the various levels of modeling problems outlined in section 1, specifically those of deterministic stresses for average-passage formulations and subgrid-scale stresses for LES, requires data with high spatial and temporal resolution. Furthermore, *the data set must be complete*, i.e. it should cover the entire flow structure within a blade passage, including hub vortices, tip region, wake structure, boundary layers on the blades, etc. To generate such data, using optical techniques one needs unobstructed view of the entire domain, at any phase angle. Also, since all optical techniques involve measurement of motion of tracers, they must be uniformly distributed in the flow-field, including the powerful vortical structures associated with tip-leakage flows. These requirements dictate the kind of facility and experimental method that is available to us at this time. The need to observe the entire flow field in fine detail requires the use of PIV (and HPIV), a method with which we have considerable experience of applications in complex geometries, including pumps (e.g. Dong et al., 1992a, b, 1997a, b; Chu et al., 1995a, b; Sinha et al., 2000a, b, 2001; Roth et al., 1999, 2001). The few other applications of PIV to flow in axial turbomachines have been severely limited by optical access and reflection problems (Bryanston-Cross et al., 1992; Tisserant & Breugelmans, 1995).

Access to the entire flow domain at any phase angle can be achieved by using a fluid and blade made of material with the same optical index of refraction. Such an arrangement would enable us to resolve the flow between the blade tip and the casing, and within boundary layers. Use of

neutrally buoyant particles prevents problems involved in seeding strong vortices, by preventing relative motion caused by centrifugal forces. Thus, the chosen facility for dealing with the problems outlined above contains liquid seeded with neutrally buoyant particles with transparent blades made with material of the same index of refraction as the fluid. The resulting facility, that has been under construction for the past three years and has been completed recently, consists of a two-stage axial pump (rotor, stator, rotor, stator), with blade-shapes that are characteristic to aircraft compressors. At this time, the favorable test conditions afforded by index matching and neutrally-buoyant particles cannot be achieved using air facilities. The shortcoming of our experimental conditions is lack of compressibility and temperature variation effects. Consequently, the flow structure is substantially different from conditions that are encountered in the first stages of high-speed compressors, where shocks dominate the flow (see e.g. Copenhaver et al., 1996). However, to answer the turbulence modeling questions raised in the previous section, it is more important to obtain full and detailed data, even if it is only relevant to the predominantly subsonic portions, such as the aft stages of compressors.

2.2 Detailed Description of the New Facility: The recently completed test facility allows detailed measurements of the velocity distribution within an entire stage, including the rotor, stator, gap between them, inflow into the rotor and the wake downstream of the stator. Sketches of the system are presented in Figures 1 - 4. Figure 1 is an overall view of the test loop. Figure 2 provides details on the pump, support structure, drive system, windows, etc.,
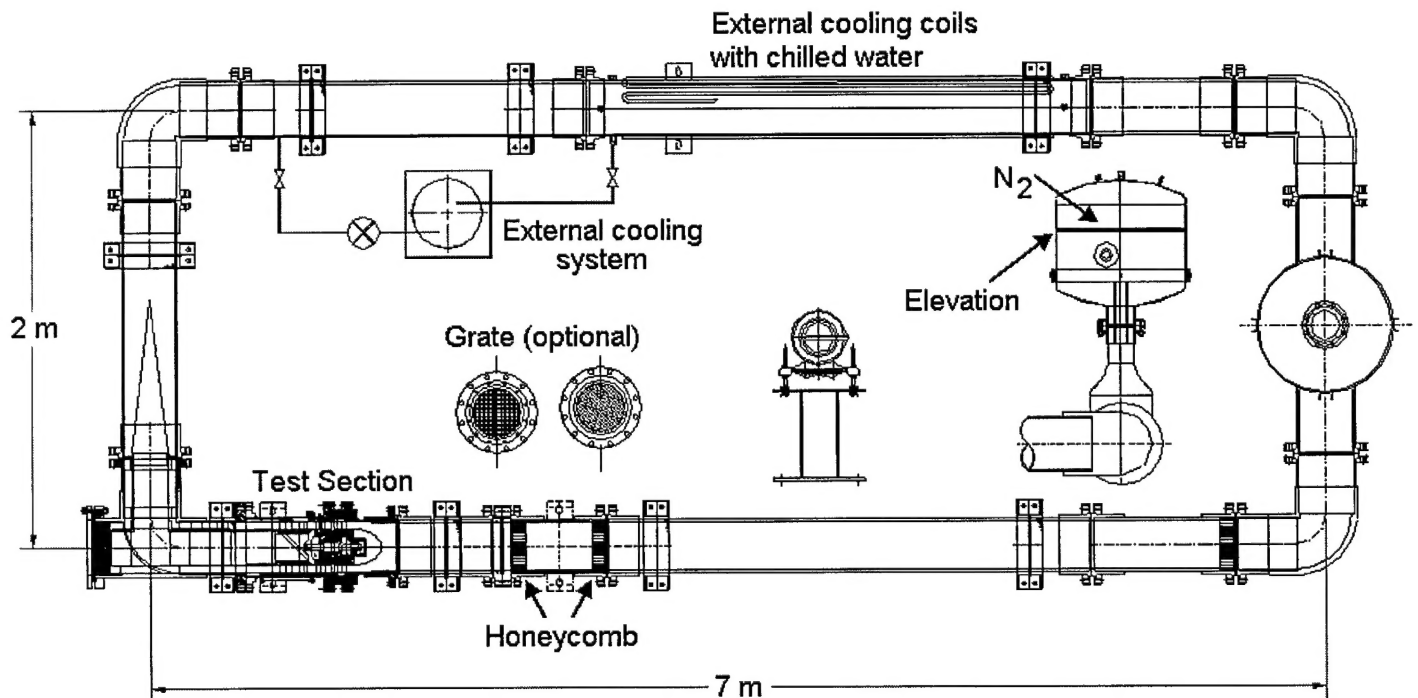
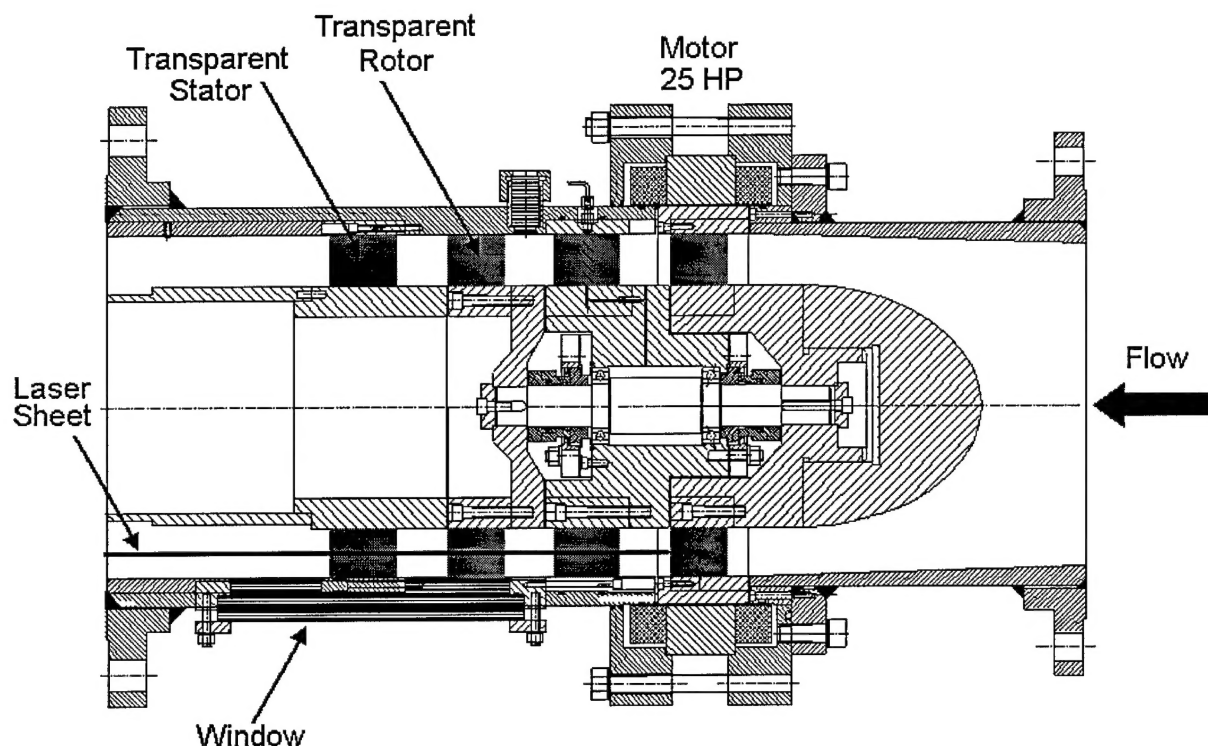Figure 1: Overall sketch of the axial turbo-pump test loop

Figure 2: The test section showing the four blade rows, location of the window, support structure, motor and bearings.

A cross section of the blades at mid span with dimensions is provided in Figure 3. The corner of the facility showing the location of the corner window and the transparent insert through which we insert the PIV illumination optics are shown in Figure 4. Several objectives are met by this design. First, this setup provides a realistic representation for flow conditions in multi-stage axial turbomachines (excluding compressibility effects) including realistic blade geometries, high Reynolds numbers and ability to vary the space between blades, including narrow gaps that characterize aircraft compressors. Second, it provides unobstructed view for 2-D PIV and 3–D holographic PIV measurements within the entire second stage, including the boundary layers on the blades, the flow around the hub and the tip leakage region. Funding for constructing this facility has been provided both by AFOSR (to deal with the modeling problems outlined in Section 2) and by ONR (to study stability, gust response and hydro-acoustics of swirling flows using different blade geometries than those shown in the present report).

The test loop (Figure 1) consists of 30.5 cm diameter pipes that contain means for generating and reducing the free stream turbulence (as required) as well as for controlling the temperature. The test section is located near one of the corners. This two - stage axial turbomachine consists of four blade rows. The two rotors have a common shaft that is supported by precision bearings immersed in a sealed oil bath. All the blade rows have an outside diameter of 30 cm and a hub diameter of 21.6 cm. The system is driven by a 25 HP rim-driven, permanent magnet, AC motor. The rotor of the motor is encapsulated in a stainless steel shell and is directly connected to the band surrounding the rotor of the first stage. The second stage is driven by the common shaft.

This drive mechanism has several advantages. First, since the system does not have a long shaft leading to an external motor it allows unobstructed illumination from the back side of any point in the second stage (details follow). Second, the direct connection to the first blade row, short hard shaft and precision bearings insure quiet and reliable operation with minimum vibrations. Third, variations in the gap between blade rows is simple and does not require modifications to the drive system.

Figure 3: The dimensions of blades at mid span.

The structure containing the bearings is held in place by the first stator. The first stage is made of metal (Naval Bronze) and the entire second stage (rotor, stator and hub) is made of acrylic. To avoid undesirable secondary flows and massive separation the 21.6 cm diameter hub extends around the corner (Figure 4) and then tapers slowly at a cone angle of 7^0. The 12" pipes are divided to several sections that enable us to insert honeycombs and screens for reducing the turbulence as well as grids for generating turbulence. Both rotors have 12 blades, each with a chordlength of 50 mm, span of 44.5 mm, thickness of 7.62 mm and camber varying between 2.54 mm at the hub to 1.98 at the tip. The stators have 17 blades, each with a chordlength of 73.2 mm, span of 44.5 mm, thickness of 11 mm and camber of 6.223 mm. The blade rows were manufactured using precision CNC machines and the surfaces were subsequently hand finished to maintain the surface roughness below 0.0076 mm. The test loop has a temperature control
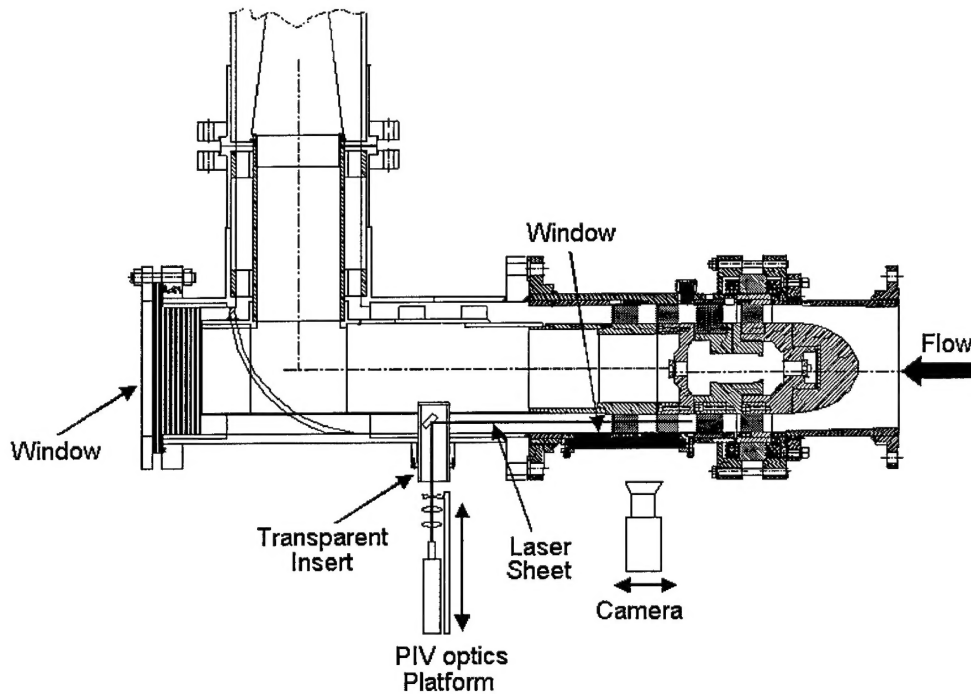
Figure 4: The corner of the facility showing the illumination port for the PIV system and the corner window.

system and provides considerable flexibility in installing other devices including pressure transducers, honeycombs and grids as well as changing blade rows.

2.3 Optical Access: Optical access is provided by a window that extends from upstream of the rotor, covers the entire second stage and terminates downstream of the stator (Figures 1-4). In addition, a large window located at the corner of the facility provides an unobstructed view in the axial direction. These windows enable us to illuminate any desired plane with a laser sheet (for 2-D PIV measurements), from the hub to the tip of the blades. The interrogated planes can be parallel or normal to the axis of the pump. The corner window also provides us with an optical access to the interior of the rotor and the stator, which is essential for 3-D, holographic PIV measurements (Zhang et al., 1997; Tao et al. 1999, 2000, 2001). As described in these references, HPIV presently enables us to record and generate an array of 128x128x128 instantaneous velocity vectors.

In order to provide unobstructed view of the flow near curved and skewed blades (and transmission of the laser sheet through blades), especially close to the hub and the tip, we use a fluid that has an index of refraction equal to that of the acrylic blades and window. Based on initial tests we opted to use water with concentrated (66% by weight) solution of NaI. This fluid has a specific gravity of 1.85 and a kinematic viscosity of 1.08×10^{-6} m^2/s (i.e. very close to that of water). The resulting Reynolds number based on the tip speed and rotor chordlength is 6.1×10^5. With this index-matched fluid the entire second stage becomes invisible, providing an unobstructed view of any point. Matching the index of the hub and the window also allows

10

unobstructed transmission of the illuminating beam of the holography system (Figure 3a). The cost of the NaI is substantial - $28,000-$30,000 to fill the entire facility. About half of the funds for the salt have been provided by the *present AFOSR DURIP grant* and the other half was provided by ONR funding. The salt has already been mixed with the water and the facility has operated with the index-matched fluid for several months. One of the difficulties that we had to overcome is the tendency of a small fraction of the I^- ions to be oxidized into I_3^- once it is exposed to light and to Oxygen. The latter absorbs green light, which complicates the PIV measurements. Experiment and testing using spectroscopy showed that limiting the exposure of the water to light, and maintaining an oxygen-free environment within the facility (the tank with the water-gas interface contains pure nitrogen) solves this problem. We did not detect any significant levels of I_3^- in the water for several months.

All of the optical elements shown in Figure 4 already exist and have been integrated with the test facility. The injection seeded Nd-YAG laser has been purchased using funds provided by a 1996 AFOSR DURIP grant. *The present AFOSR DURIP* grant provided the resources for purchasing a 15 frames/s, high resolution, 2K x 2K pixels^2, "cross correlation" digital camera (Kodak Megaplus ES4) and associated data acquisition system. The latter consists of a dual-processor PC, mass storage capacity (presently 200 GB), 2 GB RAM, image acquisition board, and software for interfacing the camera with the image acquisition system. This system can record data for extended periods at 60 MB/s. The data can either be stored on the RAM or transmitted directly to a 240 GB external hard-disc array. The new camera has already been integrated with the high-speed image acquisition system. The laser and data acquisition system are also integrated with the control system of the test facility that receives a signal from a precision shaft encoder. A delay generator enables us to record data at any desired phase of the rotor. This system overcomes the shortcomings of our previous 2kx2k, image-shifted auto-correlation digital camera (Sinha et al., 2000a, b) that has a realistic minimum delay between exposures of 50μs, which severely limits its ability to record data in the high-speed flows expected in the turbomachinery facility. It also overcomes the resolution limitation of our 1K x 1K camera, which is critical when the data is spatially filtered in order to determine the SGS stresses for LES.

We have also measured the velocity distributions at the inlet to the first stage. The mean flow appears as a classical turbulent pipe flow without any significant distortions. The performance curve of the pump has the desired/expected trends. With minimum disturbances in the loop (except for honeycombs) and when operating with water the total flow rate reaches the expected value of 019 m^3/s (3000 gpm) and a pressure rise of 65 KPa. Well below design conditions the familiar signs of stall appear, which may be used in the future for studying the flow structure in a stalled pump, as we have done in the centrifugal facility (Sinha et al., 2001). With the mixture of NaI and water that has a specific gravity of 1.8, the maximum speed our present 25 HP motor is reduced 750 rpm.

In addition to the salt, camera and image acquisition system, the present DURIP grant provided the resources for several additional items. Included are elements of the control system, shaft encoder, pressure transducer, valves (including a 30.5 cm valve used for measuring the performance of the facility), connectors, auxiliary pumps (for filtration and cooling) and associated pipes. These funds enabled us to complete the construction of this facility.

3. Preliminary Results:

Measurements of the flow structure and turbulence around the rotor and stator blades are currently in progress. Some of the results have already been included in two conference papers (Uzol et al., 2001; Chow et al., 2001). This section presents sample images and velocity distributions. Figure 5 is a superposition of images with the impeller located at 10 at different positions. The flow is illuminated by a single light sheet from the left and the traces are the intersections of the sheet with the rotor and stator blades at ten different phases. As is evident, the same sheet penetrates through blades and maintains its shape. The slight variations in beam intensity, which occur due to very small differences in refractive index, do not have significant effects on the quality of the PIV images. They disappear after image enhancement and we can obtain a complete data set over the entire flow field. To maintain a desired resolution we divide the flow field to five sample areas, as illustrated in Figure 6. Each covers 50x50 cm and together they cover the entire second stage, from the inlet to the rotor to the wake behind the stator. A sample original PIV image (one of the two exposures) near the trailing edge of the rotor is presented in Figure 7a. After enhancement and removal of the blade trace, the same image is shown in Figure 7b. The enhancement procedures are described in Roth and Katz (2001) with modifications that enable us to recover the particle traces very close to the surface and remove the traces of the blade.
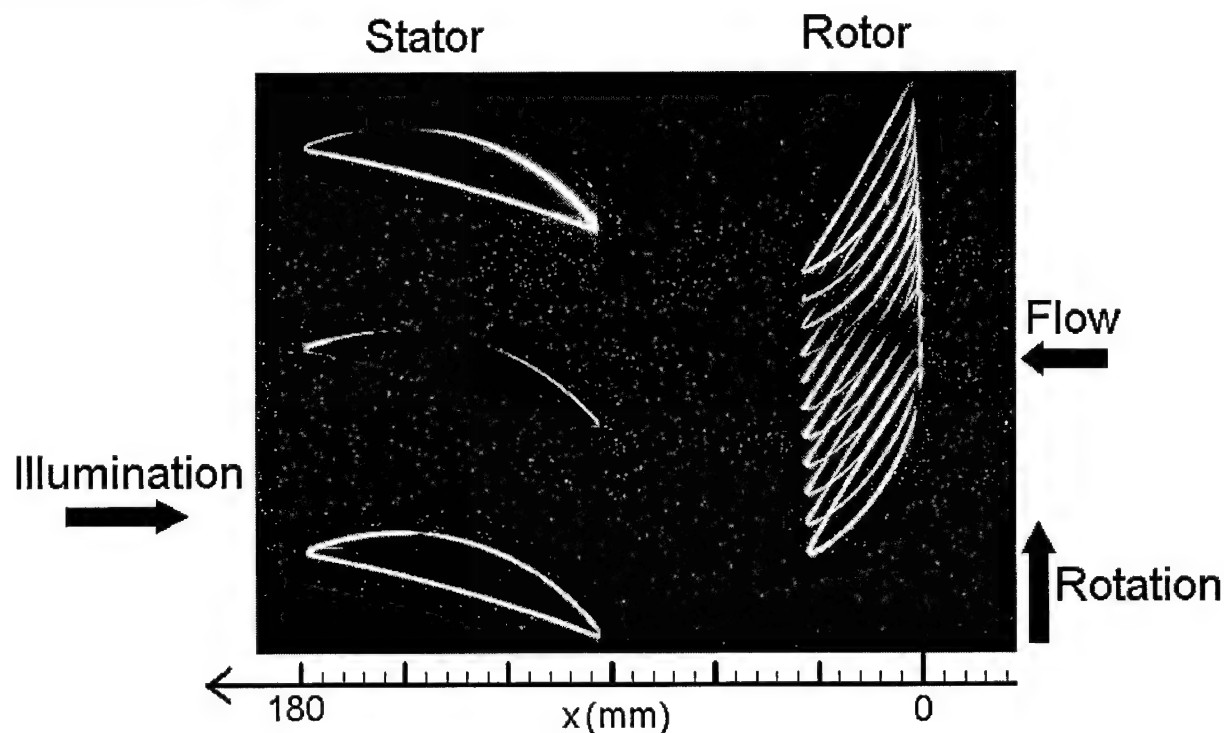
Figure 5: Superimposed images at 10 different rotor phases at 500 rpm and at the mid-span location. x=0 is defined as the rotor leading edge. The total stage length is L_S = 203 mm. Illumination is from the left and one light sheet illuminates both blade rows.
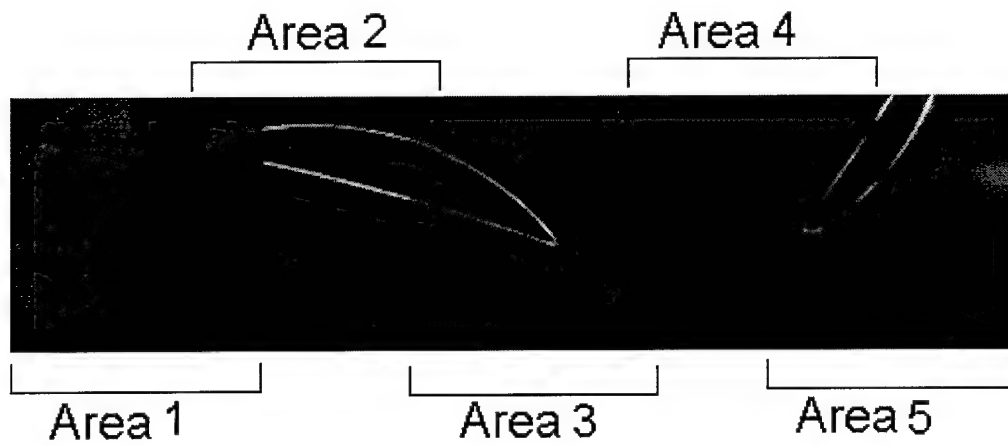
Figure 6: Sample areas used in the present experiments covering the entire stage. The size of each area is 50x50 mm. There is an intentional wider overlap between areas at the trailing edge of the blades. The purpose of this overlap is to obtain a continuous record on the development of the wake from the boundary layer, and to avoid having to cut this boundary layer in the area covering most of the blade.
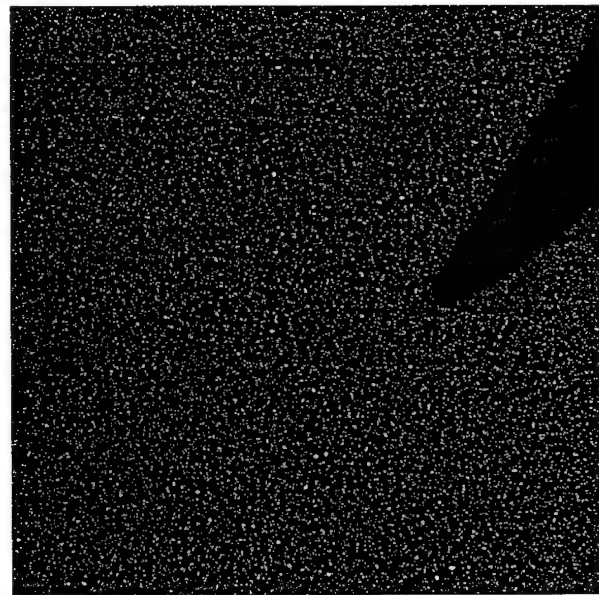
(a) Original Image   (b) Enhanced Image

Figure 7: Sample (a) original and (b) enhanced PIV images (one exposure) of the trailing edge of the rotor.

13

For each of the rotor phases (orientations) we obtained phase-averaged velocity distributions by averaging 100 instantaneous distributions. The turbulent fluctuation is defined as the difference between the instantaneous and phase averaged data. We estimate the turbulent kinetic energy based on the available velocity components as $k = 3/4(u'^2 + v'^2)$. The coefficient is based on the assumption that the variance of the out-of-plane component is equal to the average of the two in-plane components. In some cases, in order to insure that the statistics of the turbulence parameters is converged we record 1000 instantaneous realizations. So far we have recorded a complete data set in three planes, one close to the hub, the second in mid-span and the third near the tip. We have also recorded sample data in the tip gap, i.e. between the tip of the rotor and the window. Data analysis is still in progress and the results below summarize our progress.

Combining the data from all the sample areas in mid span for one of the rotor phases, one obtains the distributions the velocity and turbulent kinetic energy shown in Figure 8. Clearly, the index matched test facility enables us to perform complete and unobstructed turbulence and velocity
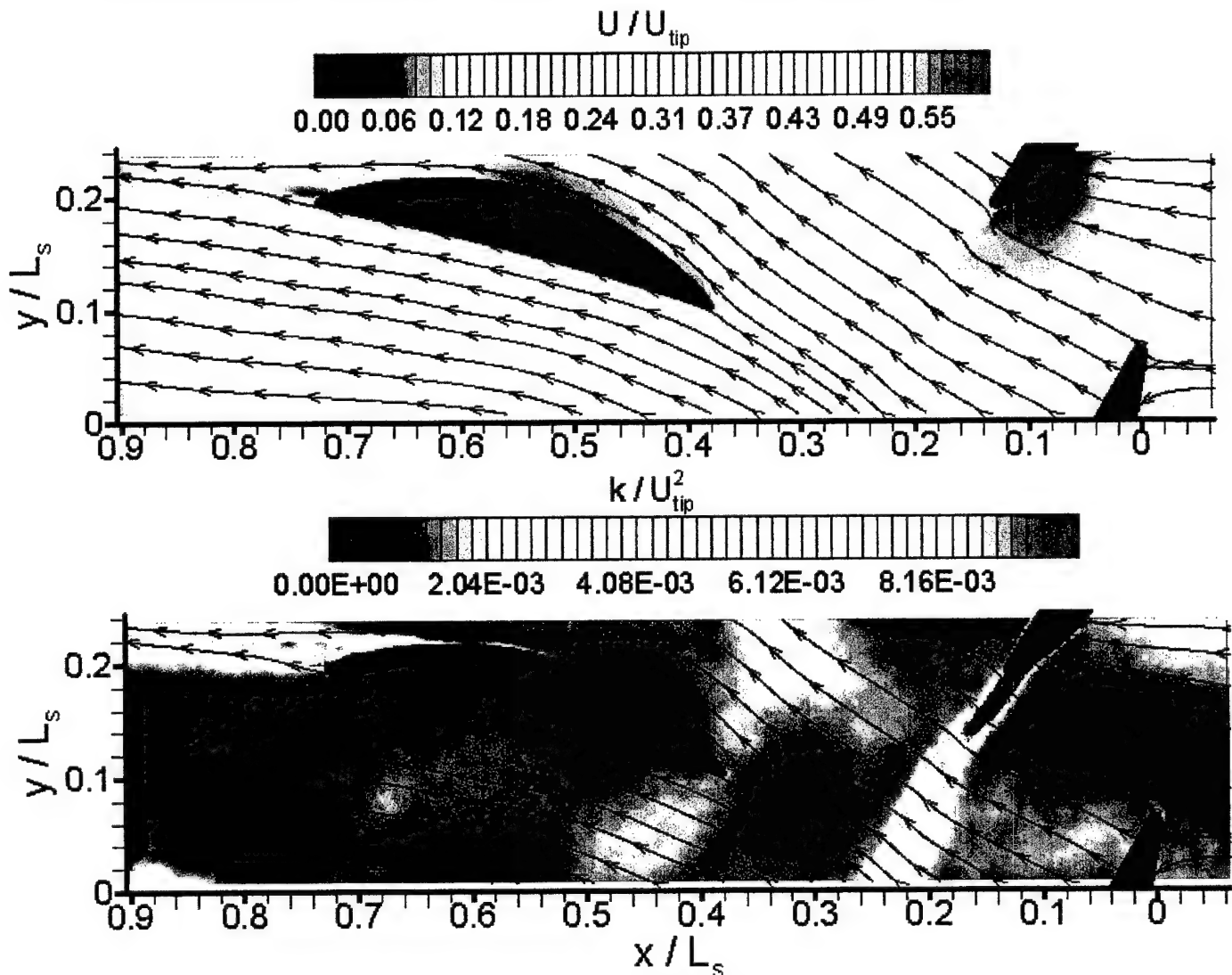
Figure 8: Distributions of (a) phase-averaged velocity and (b) turbulent kinetic energy over the entire stage at mid span along with selected streamlines.

measurements over the entire stage. The distributions of turbulent kinetic energy are dominated by wakes of the rotor blades, of the stator and even of the stator blades located upstream of the sample area (see on the right side). As will be shown shortly, these wakes have dominant effects on the flow around downstream blade rows.
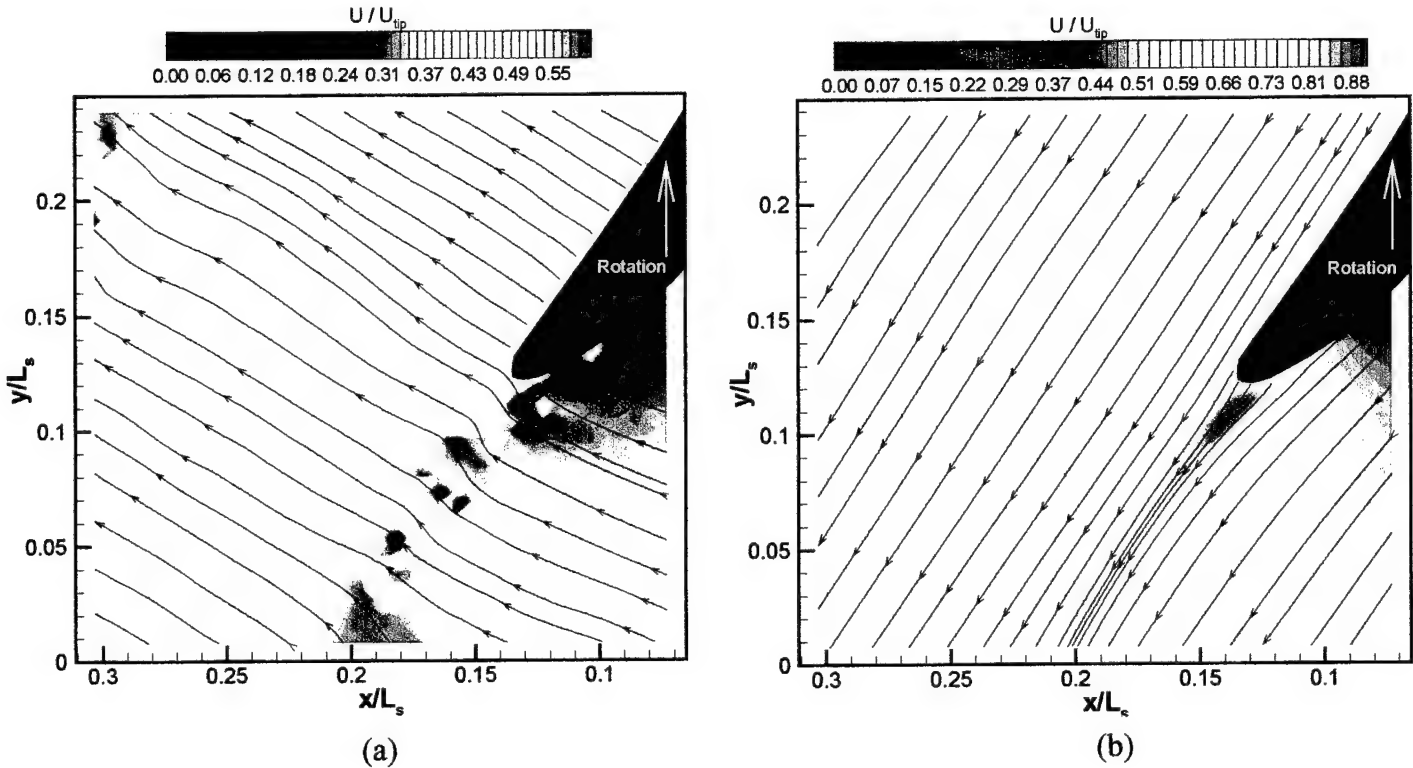

Figure 9: Sample (a) instantaneous along with the absolute streamlines, and (b) phase averaged velocity distributions along with the relative streamlines near the trailing edge of the rotor.

Focusing on the flow around the rotor figure 9 contains sample instantaneous and phase averaged velocity distributions near the trailing edge of the rotor. The mean flow is attached and the presence of the wake is clearly evident. A series of phase averaged velocity distributions along with the turbulent kinetic energy for five different rotor phases are presented in Figure 10. They show how the blade "scoops" the turbulent wake generated by the stator located upstream. In phase 8 the wake coincides with the leading edge of the rotor blade and as the blade progresses the region with elevated turbulence appears further downstream along the pressure side of the blade. Non-uniformities in the mean flow on both sides of the rotor that are associated with the upstream wake are also evident. Away from the vicinity of the blade (e.g. downstream) the mean velocity is clearly higher in regions that coincide with low turbulence levels, i.e. out side of the (upstream) stator wake. Clearly, the effect of this stator persists downstream of the following blade row. In some cases (compare phases 8 to 10) the variations in mean velocity distribution are substantial. In fact, the impact of the upstream stator can be sensed even downstream of the second stator, i.e. two blade rows downstream.
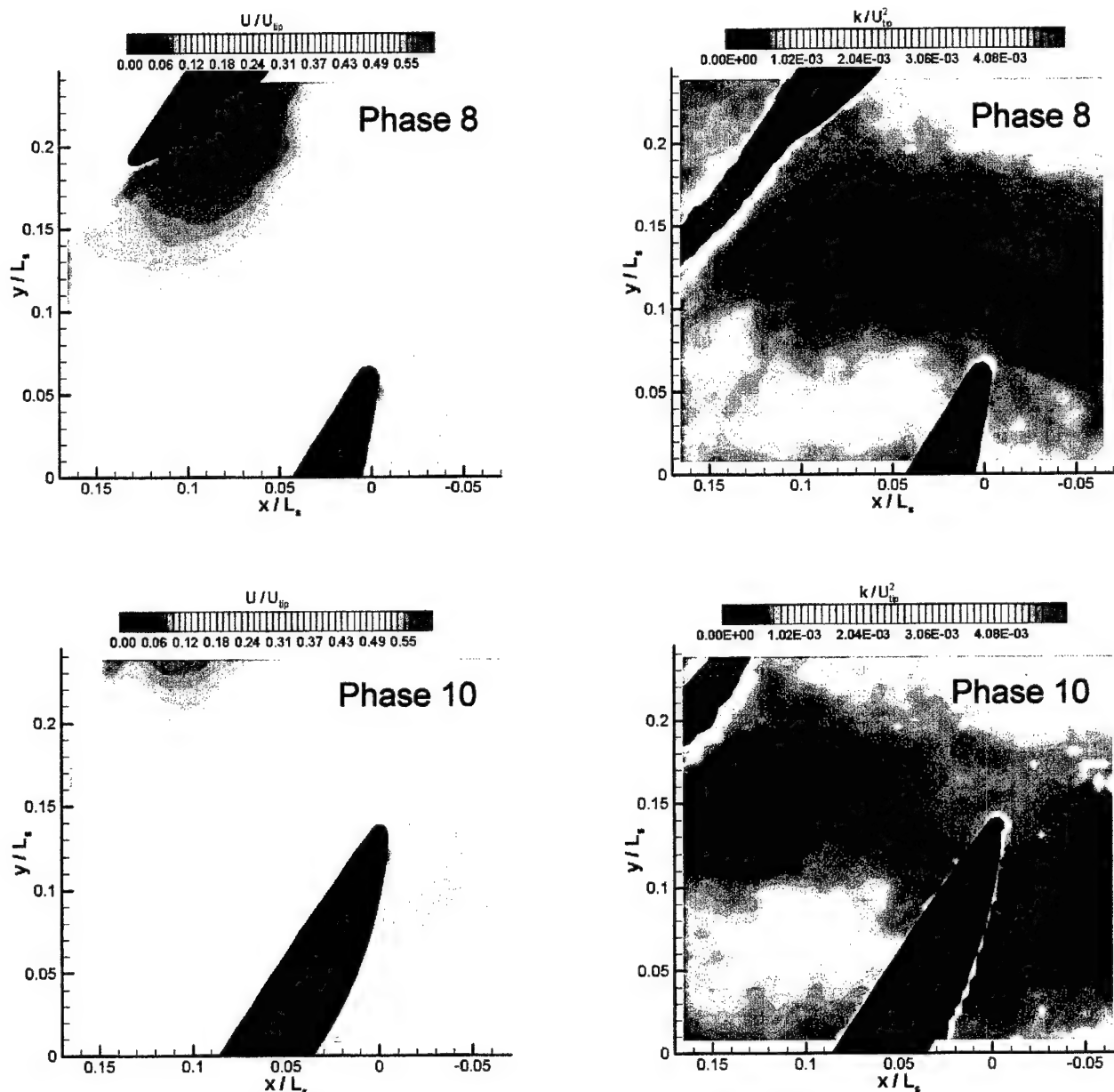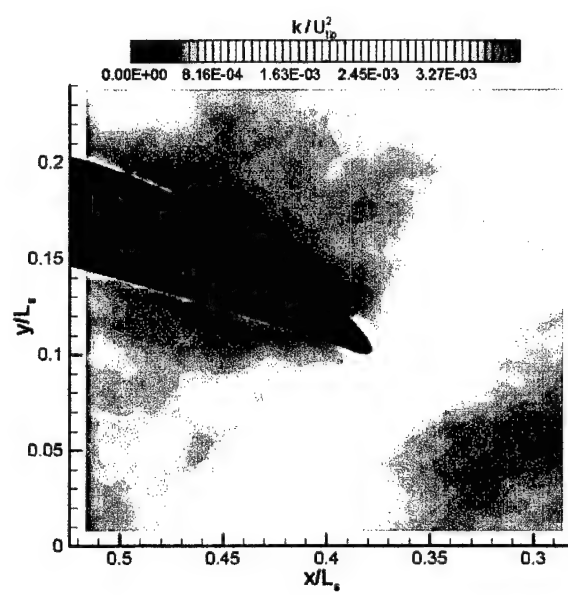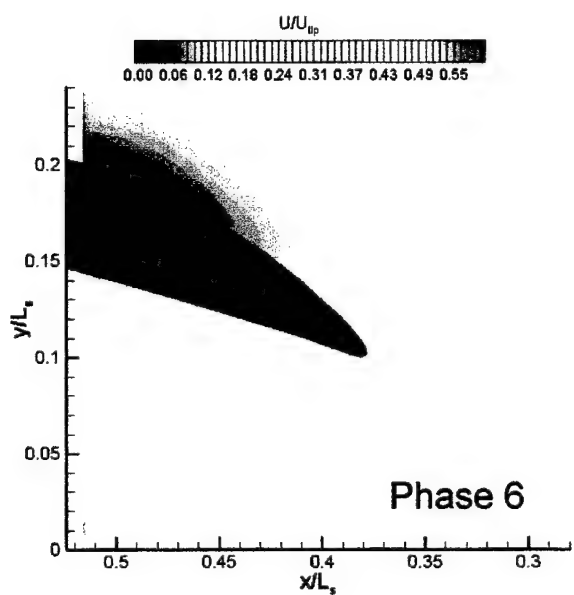
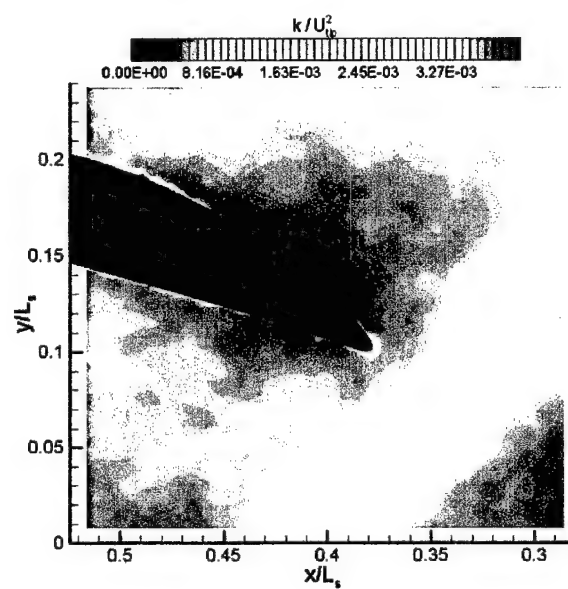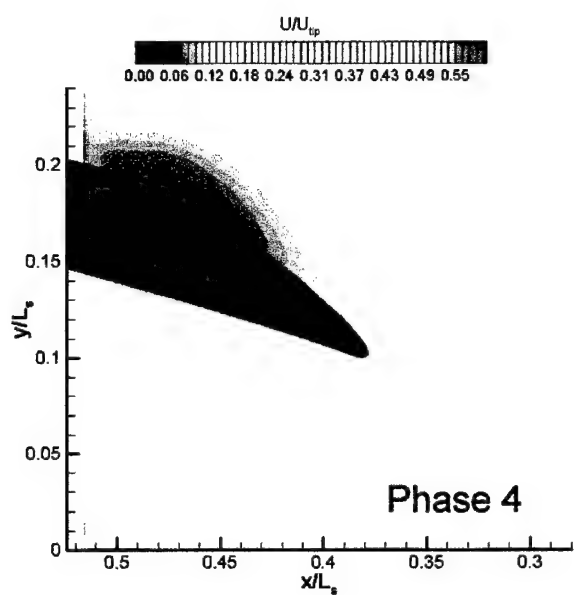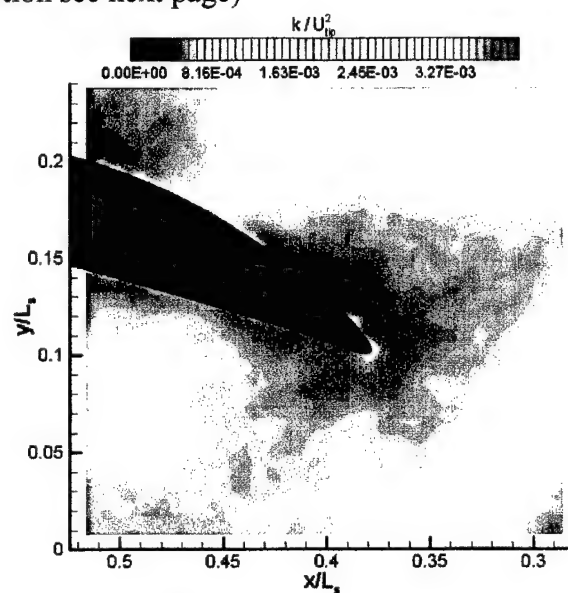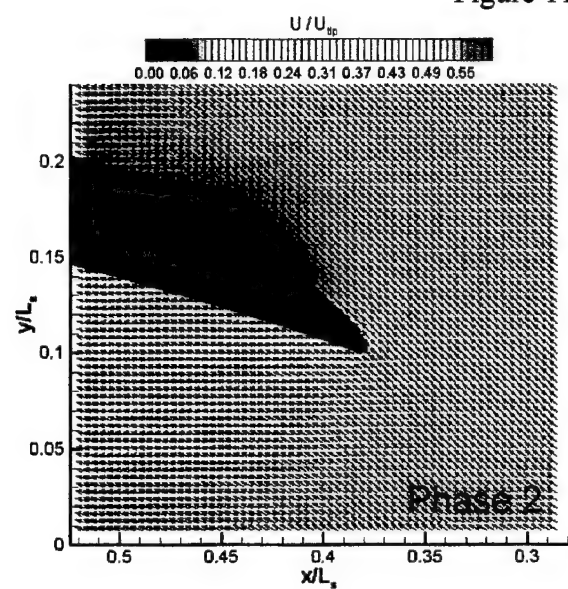Figure 10 (for caption see next page)
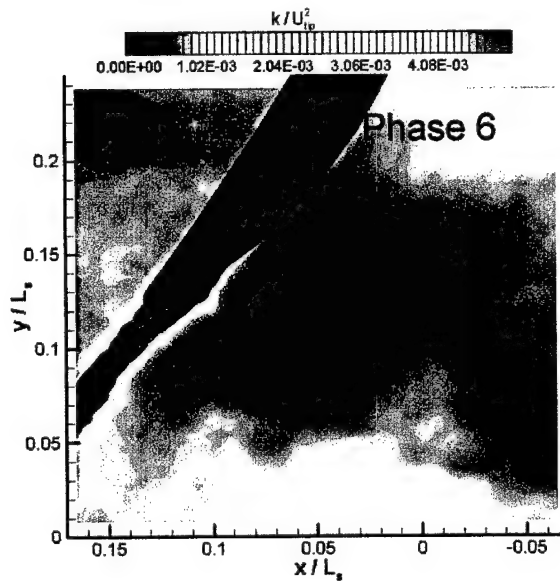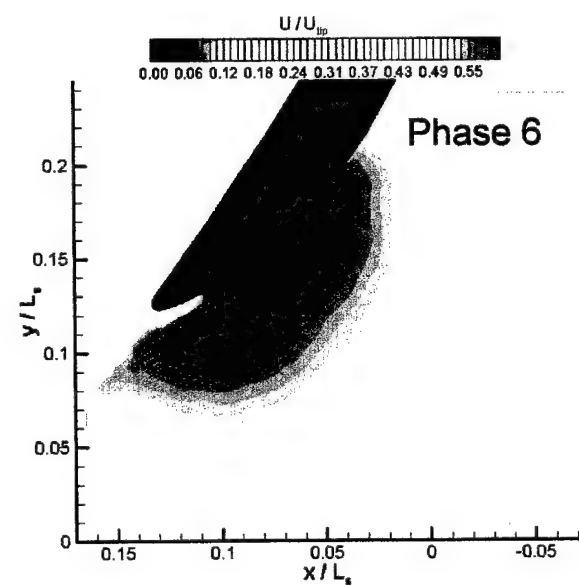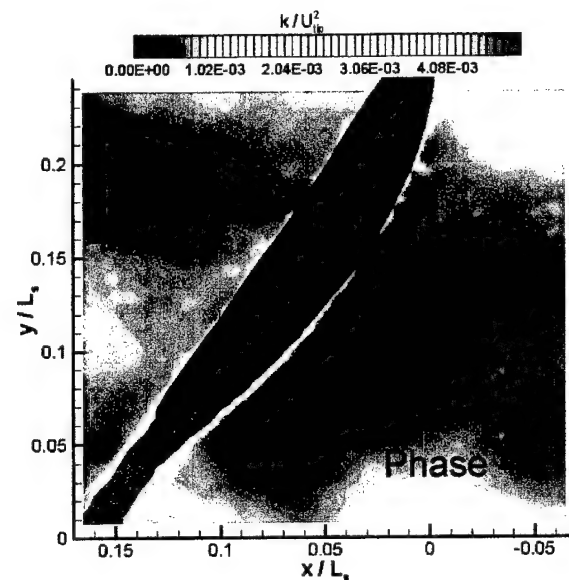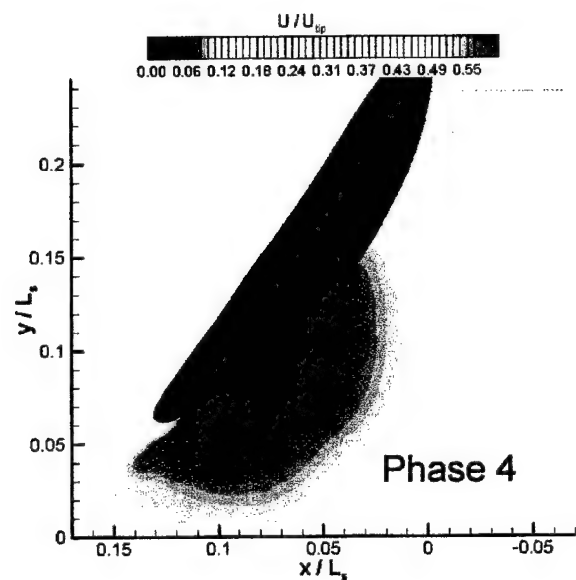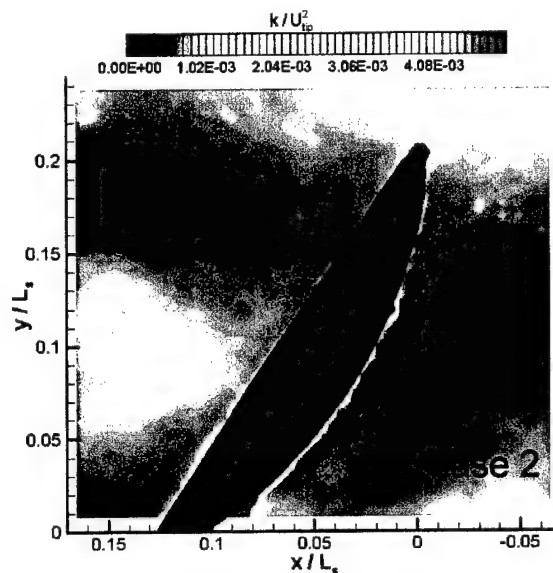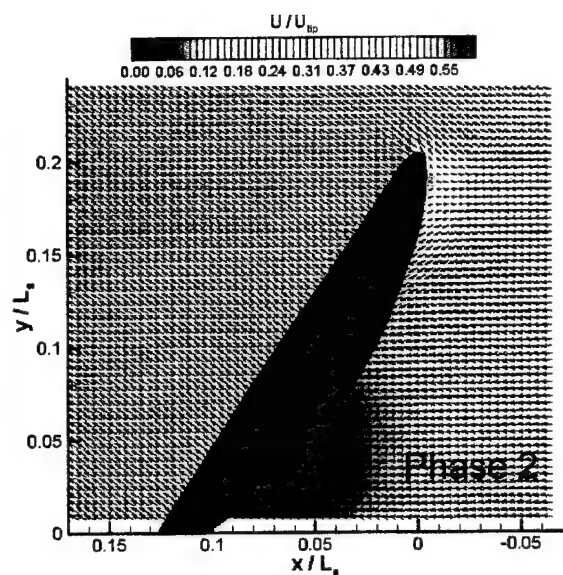
Figure 10 (continued): Phase averaged velocity and turbulent kinetic energy fields in the vicinity of the rotor for five different impeller phases (500 rpm, mid-span).

Figure 11 is a second series of phase averaged velocity and turbulent kinetic energy distributions that focuses on the leading edge of the (second) stator. As is evident, the flow is dominated by the impact of the rotor wake. The mean velocity on the right hand side of each distribution peaks within the wake of the rotor. As the wake "impinges" on the surface of the stator it causes significant changes in the velocity near the surface, predominantly on the suction side. In phases 8 and 10 the local maximum in velocity nearly coincides with the points with maximum turbulence level, but not in phases 2-6, before the wake impinges on the surface. Less obvious

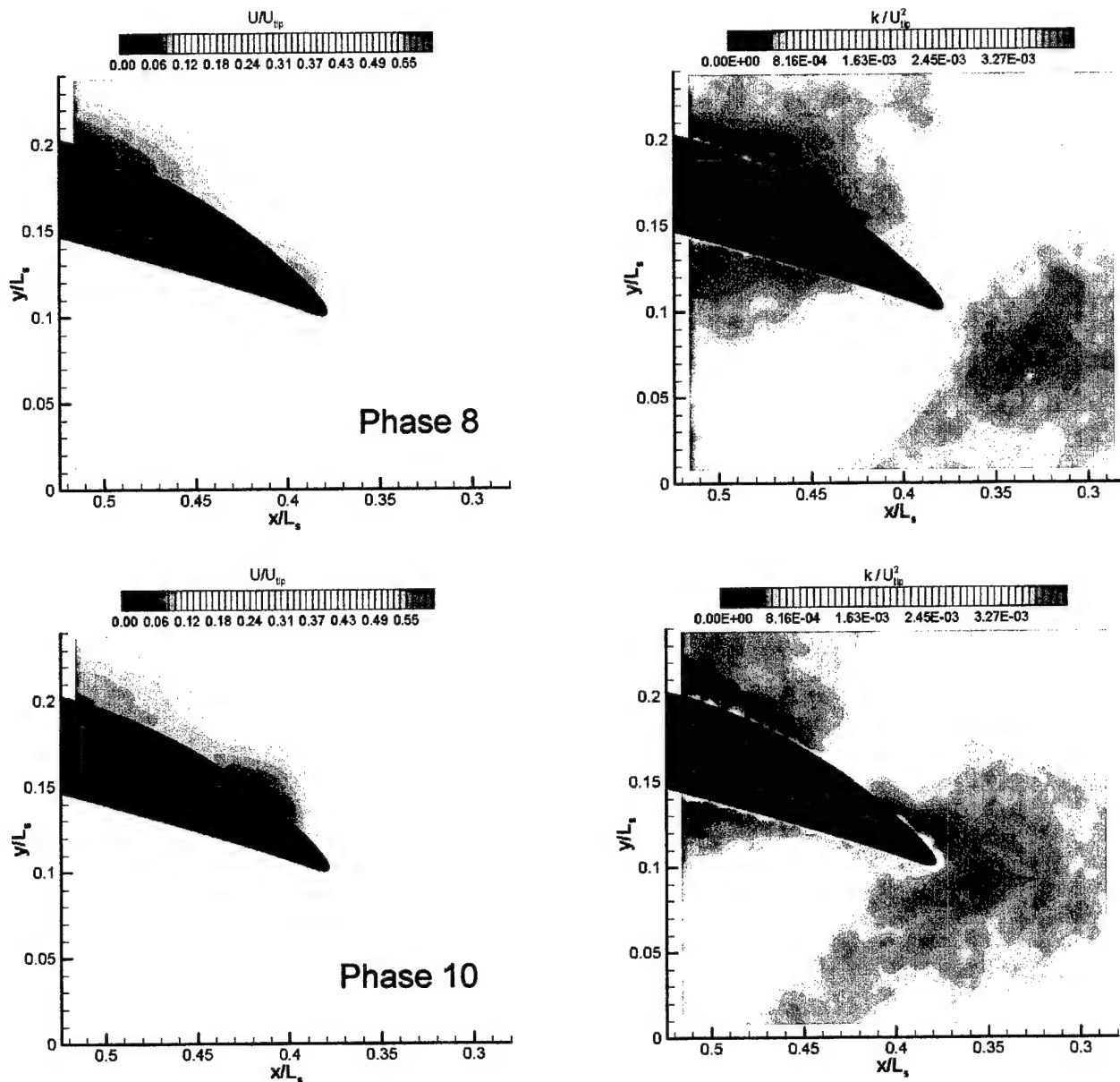Figure 11 (for caption see next page)

Figure 11 (continued): Phase averaged velocity and turbulent kinetic energy fields around the leading edge of the rotor for five different impeller phases (500 rpm, mid-span).

but still clearly noticeable is the wake of the first stator. It appears, for example in phases 2 and 4 as nearly horizontal layers with elevated turbulence levels, one near the upper boundary of the map and the other below the pressure side of the blade. Above the blade the wake of the previous stator also causes reduction in the phase-averaged velocity. Below the blade it is difficult to detect this effect. In the other phases the presence of and interaction with the rotor wake makes the stator wake less obvious but they still exist. These phase dependent variations in mean flow resulting from interactions between wakes of different blade rows and between wakes and blades would be primary contributors to the deterministic stress. The distributions of deterministic

stresses will be calculated once the data analysis is completed following the procedures described in Sinha et al. (2000).

Finally, measurements at higher magnification can be used for characterizing the flow within the boundary layers. For example, Figures 12 and 13 are the velocity distributions near the trailing edge of the stator. Substantial thickening of the boundary layer but no reverse flow occur in both the mean and instantaneous velocity distributions. This thickening is also evident from Figure 8. The instantaneous map shows the expected intermittent entrainment of external fluid into the boundary layer. Plotting three characteristic mean velocity distributions show the substantial increase in the boundary layer thickness and the formation of an inflection point in the velocity profile. The latter is expected to occur in regions with adverse pressure gradients, when the boundary layer is about to separate. Associated with this trend is a substantial increase in the turbulent kinetic energy that peaks at the inflection point.

Figure 12: Instantaneous velocity distribution of the stator boundary layer near its trailing edge ($c_S = 73.15$ mm is the stator stator chordlength)
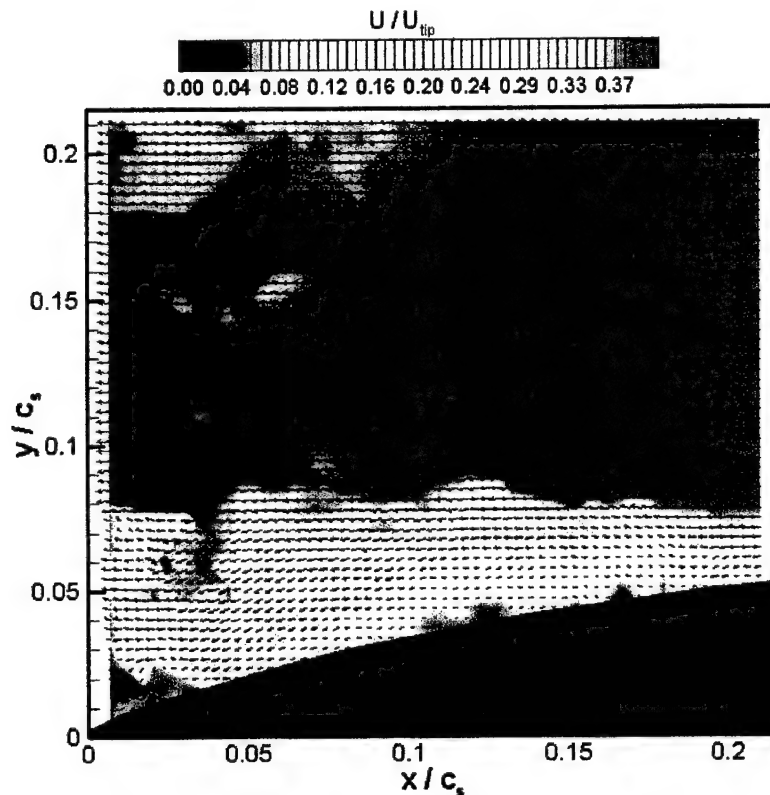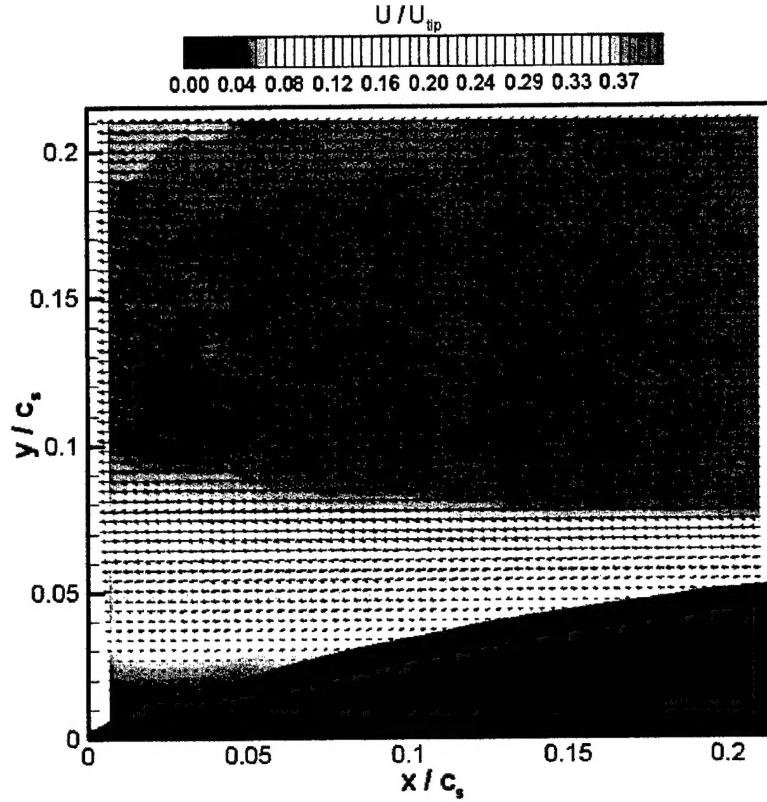
Figure 13: Phase average velocity field of the stator boundary layer near its trailing edge (c_S = 73.15 mm is the stator chordlength).
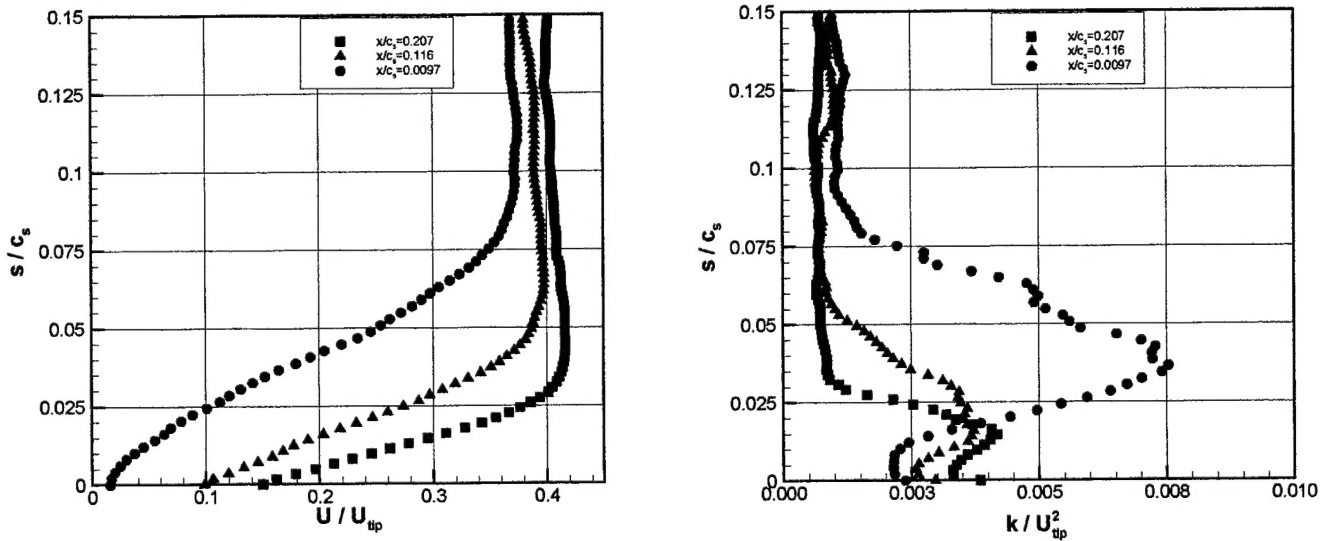

Figure 14: Phase averaged velocity (U) and turbulent kinetic energy profiles in the stator boundary layer (s is the distance from the blade surface, U_{tip} = 8 m/s).

4. Future Plans:

The research described in this report is still in progress under a recently awarded new AFOSR grant. Using the equipment provided under the present DURIP grant we have already recorded data in three planes, near the hub, at mid span (samples have been shown) and near the tip. Some of the results have already been presented in two conference papers (Uzol et al., 2001; Chow et al., 2001). We are also in the process of assembling a stereo-PIV system for measuring the distributions of all three velocity components in the illuminated planes. In the future we will also perform measurements of surface shear stresses and pressure fluctuations within the (second) stage of the index-matched axial turbomachine facility. The data will be used for addressing turbulence-modeling issues that are relevant to flows within turbomachines, as outlined in Section 2 of this report. Specific tasks are:

a. We will complete the analysis to obtain a complete 2-D PIV data-base covering the entire second stage in three planes at ten different rotor phases.
b. The data will be used for calculating the distributions of deterministic and Reynolds stresses.
c. Subsequent analysis will focus on specific contributors to the phase dependent variations in flow/turbulence structure.
d. High resolution and high magnification measurements will be performed (some are already completed) in selected regions, such as boundary layers, providing 128x128 vectors per instantaneous realization with vector spacing of 120 µm. The resulting data sets will enable spatial filtering and calculations of subgrid stresses for LES.
e. Using an array of MEMS based wall shear stress sensors mounted on the surface of a stator blade, and flush mounted pressure transducers, we also plan to perform simultaneous wall stress and PIV (and selected HPIV) measurements in selected phases.
f. Subsequent data analysis will include calculations of the phase averaged velocity, pressure, and shear-stress distributions, Reynolds stresses, turbulent kinetic energy and deterministic stresses, spatially filtered, large-scale flow fields as well as distributions of subgrid stresses for LES.
g. Using spatial spectra we will estimate the distributions of dissipation rates, that together with the kinetic energy will provide the RANS community with detailed data on parameters typically used for Reynolds stress modeling.
h. In the context of average-passage modeling the analysis will focus on the effects of interactions between blade rows on the deterministic stresses. Included are, for example, wake, tip leakage and hub vortex interactions with downstream boundary layers, as well as boundary layer separation and "wake flutter" caused by a non-uniform velocity and pressure distributions at the exit (or entrance) from (or to) a neighboring blade row. Also, as illustrated in this report, interactions between wakes should have significant effects on the deterministic stresses.
i. The effort to model the measured deterministic stresses will continue. For example, we will continue to evaluate a successful approach to estimate the deterministic stresses (Meneveau and Katz, 2001) that relies on a limited number of steady RANS with phase-dependent, non-uniform inflow conditions.
j. In the context of subgrid scale (SGS) stress modeling for LES, the measured stresses will be compared to model predictions at different scales, including eddy-viscosity, similarity and dynamic models. Specific problems, such as those related to boundary layer separation or

rapid straining, will be identified and effort will be made to propose modifications to these models that would address these problems.

k. Still in the LES context, efforts will be made to develop models that will address the relationships between the filtered unsteady velocity field near the stator blade and the wall shear stresses. Questions as to the validity of using RANS based wall stresses as boundary conditions for LES will be addressed.

References:

Adamczyk, J.J. 1985 Model Equation For Simulating Flows In Multistage Turbomachinery. *ASME Paper No.*, 85-GT-226.

Adamczyk, J.J., Celestina, M.L., Beach, T.A., & Barnett, M. 1990 Simulation Of Three-Dimensional Viscous Flow Within A Multistage Turbine. *ASME J. Of Turbomachinery*, **112**, 370.

Adamczyk, J.J., Celestina, M.L., & Chen, J.P. 1996 Wake Induced Unsteady Flows: Their Impact on Rotor Performance and Wake Rectification, *J. Turbomachinery*, **118**, 88.

Adkins, G.G. & Smith, L.H. 1982 Spanwise Mixing In Axial-Flow Turbomachines. *ASME J. Of Engineering Power*, **104**, 97.

Bryanston-Cross, P.J., Towers, C.E., Judge, T.R., Towers, D.P., Harasgama, S.P., Hopwood, S.T., 1992, "The Application of PIV in a Short Duration Transonic Annular Turbine Cascade," ASME J. of Turbomachinery, 114:504.

Busby J., Sondak D., Staubach B & Davis R. 2000 Deterministic Stress Modeling of a Hot Gas Segregation in a Turbine. *J. Turbomachinery* **122**, 62.

Chow, Y.C., Uzol, O., Katz, J., & Meneveau, M. 2001 An Investigation of Axial Turbomachinery Flows Using PIV in an Optically-Unobstructed Facility. Submitted to The 9th Int. Symp. on Transport Phenomena and Dynamics of Rotating Machinery (ISROMAC 9), Honolulu, Hawaii, February 10-14, 2002.

Chu, S., Dong, R. & Katz, J. 1995a Relationship Between Unsteady Flow, Pressure Fluctuations And Noise In A Centrifugal Pump. Part A: Use Of PIV Data To Compute The Pressure Field. *J. Of Fluids Engineering*, **117**, 24

Chu, S., Dong, R. & Katz, J. 1995b Relationship Between Unsteady Flow, Pressure Fluctuations And Noise In A Centrifugal Pump. Part B: Effect Of Blade-Tongue Interaction. *J. Of Fluids Eng*, **117**, 30

Copenhaver W.W., Mayhew M.M., Hah, C. and Wadia, A.R., 1996 The effect of tip clearance on a swept transonic compressor rotor, *ASME J. Turbomachinery* **118**, 230.

Dawes, W.N. 1992 Towards improved throughflow capability: the use of three-dimensional viscous flow solvers in a multistage environment, *ASME J. of Turbomachinery* **114**, 8

Denton J.D., 1992 The calculation of three-dimensional viscous flow through multistage turbomachines *ASME J. of Turbomachinery* **114**, 18.

Dong, R., Chu, S., & Katz, J. 1992a, Quantitative Visualization Of The Flow Structure Within The Volute Of A Centrifugal Pump, Part A: Technique." *J. Of Fluids Eng.*, **114**, 390.

Dong, R., Chu, S., & KATZ, J. 1992b, Quantitative Visualization Of The Flow Structure Within The Volute Of A Centrifugal Pump, Part B: Results And Analysis. *J. Of Fluids Eng.*, **114**, 390.

Dong, R., Chu, S., Katz, J., (1997), "Effect of Modification to Tongue And Impeller Geometry on Unsteady Flow, Pressure Fluctuations and Noise in A Centrifugal Pump", *ASME Journal of Turbomachinery*, Vol. 119, pp. 506-515.

Dong, R., Katz, J., Huang, T.T., (1997), "On The Structure of Bow Waves on A Ship Model," *Journal of Fluid Mechanics*, Vol. 346, pp. 77-115.

Gallimore, S.J. & Cumpsty, N.A. 1986 Spanwise Mixing In Multistage Axial Flow Compressors: Part I - Experimental Investigations. *ASME J. Of Turbomachinery*, **108**, 2.

Ho, Y.H. & Lakshminarayana, B. 1995 Computations of Unsteady Viscous Flow Through turbomachinery Blade Row Due to Upstream rotor Wakes. *J. Turbomachinery*, **117**, 541.

Kirtley, K.R., Beach, T.A., & Rogo, C. 1993 Aeroloads And Secondary Flows In A Transonic Mixed-Flow Turbine Stage. *ASME J. Of Turbomachinery*, **115**, 590.

Lakshminarayana, B. 1991 An Assessment Of Computational Fluid Dynamic Techniques In The Analysis And Design Of Turbomachinery - 1990 Freeman Scholar Lecture. *J. Of Fluids Eng*, **113**, 315.

Lejambre, C.R., Zacharias, R.M., Biederman, B.P., Gleixner, A.J., & Yetka, C.J. 1998 Development And Application Of A Multistage Navier-Stokes Solver. Part II: Application To A High Pressure Compressor Design, *ASME J. Turbomachinery* **120**, 215.

Lesieur, M. & Metais, O. 1996 New Trends In Large-Eddy Simulations Of Turbulence. *Annu. Rev. Fluid Mech.*, **28**, 45--82.

Liu, S., Katz, J. & Meneveau, C 1999 Evolution And Modeling Of Subgrid Scales During Rapid Straining Of Turbulence. J. Fluid Mech. **387**, 281.

Meneveau, C. 1993 Statistics of turbulence subgrid-scale stresses: Necessary conditions and experimental tests *Phys. Fluids A* **6** 815.

Meneveau, C. & Katz, J., 2000, Scale-invariance and turbulence modeling for Large Eddy Simulation. *Annual Rev. Fluid Mech.* **32**, 1-32.

Uzol, O., Chow, Y.C., Katz, J., & Meneveau, M. 2001 Unobstructed PIV Measurements within an Axial Turbo-Pump Using Liquid and Blades with Matched Refractive Indices. 4th Int. Symp. on Particle Image Velocimetry, Göttingen, Germany, September 17-19.

O'Neil, J. & Meneveau, C 1997 Subgrid-Scale Stresses And Their Modeling In The Turbulent Plane Wake, *J. Fluid Mech.*, **349**, 253.

Rai, M.M. 1987 Navier-Stokes Simulation Of Rotor/Stator Interaction Using Patched And Overlaid Grids. *J. Of Propulsion And Power*, **3**, 387.

Rhie, C.M., Gleixner, A.J., Spear, D.A., Fischberg, C.J., & Zacharias, R.M. 1998 Development and Application Of A Multistage Navier-Stokes Solver. Part I: Multistage Modeling Using Body Forces and Deterministic Stresses. *ASME J. Turbomachinery* **120**, 205.

Rogallo, R. & Moin, P. 1984 Numerical Simulation Of Turbulent Flows. *Ann. Rev. Fluid. Mech.,* **16**, 99.